29.0 IDENTIFICATION OF DEFORMATION MECHANISMS IN THERMALLY STABLE CAST AL-CU ALLOYS *VIA* NEUTRON DIFFRACTION

Brian Milligan (Mines)
Faculty: Amy Clarke (Mines)
Other Participants: Francisco Coury (Mines)
Industrial Mentor: Amit Shyam (ORNL)

This project initiated in Fall 2017 and is supported by the Colorado School of Mines (Mines) and Oak Ridge National Laboratory (ORNL). The research performed during this project will serve as the basis for a Ph.D. thesis for Brian Milligan.

29.1 Project Overview and Industrial Relevance

Cast Al-Cu alloys have long been popular in applications that require complex shapes, low density, and high strength. One such application is cylinder heads for internal combustion engines. However, as temperatures in commercial engines increase, the precipitates in these alloys begin to coarsen and transform during service. This leads to a loss of strength [29.1], due to a larger precipitate spacing [29.2] and a change in deformation mechanisms [29.3, 29.4].

In order to fully understand and improve mechanical properties, characterization at grain size length-scale is required. This work includes neutron diffraction experiments combined with synchrotron x-ray imaging and transmission electron microscopy (TEM) experiments to understand the role of grain orientation and precipitate size/morphology on the mechanical properties.

29.2 Previous Work

29.2.1 Literature Review

Al-Cu precipitation has been studied in detail and generally follows the transformation pathway: supersaturated solid solution → plate-shaped, single atomic layer Guinier-Preston (GP) I zones → plate-shaped, 2-4 layer GPII/θ″ precipitates → thick, plate shaped θ′ precipitates → approximately spherical or rod-shaped θ equilibrium precipitates [29.2]. Yielding and strain hardening behavior in polycrystalline alloys have long been a popular area of study [29.5]. With modern computational tools and experimentation, models to describe these quantities are being continually refined. Of particular interest is the work of da Costa Teixiera *et al.*, who improved the accuracy of yielding and strain hardening models for Al-Cu alloys by avoiding the common simplifying assumption of spherical precipitates [29.3, 29.4]. Another recent development is the application of self-consistent models [29.8] to describe the deformation behavior of polycrystals, without the assumptions made by the classical models of Taylor and Sachs [29.5].

In order to observe the effect of applied stress on precipitate shearing behavior, early models of precipitate rafting behavior were studied [29.6]. It was hypothesized that the interface behavior is similar in these two situations. In these works, it was concluded that lattice mismatch between precipitate and matrix phases can be aggravated or reduced by the application of external stress, as demonstrated in **Figure 29.1**. An understanding of the precipitate shear plane interface is also helpful in the development of this model, and is described in [29.7].

29.2.2 Identification of Deformation Mechanisms *via* Neutron Diffraction

Following the analysis of da Costa Teixiera *et al*, precipitates may still be shearable at greater thickness than previously considered. The work from da Costa Teixiera *et al* implies that the θ′ precipitates in most of the alloys and conditions evaluated in this study are shearable. In order to study the dislocation-precipitate interactions, lattice strain (measured as the change in lattice spacing, which can be related to stress within the crystal) is compared to macroscopic strain in a tensile specimen using in-situ neutron diffraction of four lattice planes, each corresponding to a different grain orientation, for four aging conditions of 206 Al. These results can be seen in **Figure 29.2**. This relationship can be thought of as a stress-strain curve for individual families of grain orientations.

Figure 29.2 displays a distinct change in strain hardening behavior as precipitates grow in thickness. Particularly, anisotropy between strain hardening behaviors in different grains arises in the peak aged and 200°C overaged conditions, suggesting that these conditions are in a transition regime between two deformation mechanisms, with individual grain orientations controlled by one or the other mechanism.

The two mechanisms that control strain hardening in these conditions are related to whether dislocations shear through precipitates or loop around them. Whether dislocations shear or loop around precipitates depends primarily on the size and coherency of the precipitates. **Figure 29.3** shows scanning transmission electron microcopy (STEM) high angle annular dark field (HAADF) micrographs (a,c) and dark field (DF) (b) of Cu rich precipitates in the peak aged, 200 °C overaged, and 300 °C overaged conditions. Although not shown in **Figure 29.3,** the thin GP zones of the natural aged sample allow for precipitate shearing to be the dominant mechanism. The thick, incoherent precipitates of the 300°C overaged condition allows for Orowan looping to be dominant. The peak aged and 200°C overaged conditions have intermediate precipitate thicknesses that could undergo either mechanism.

29.3 Recent Progress

29.3.1 Quantitative Model for Precipitate Shearing Energetics

In order to describe the transition from shearing or Orowan looping, an energetic analysis of the newly-created interface post-shearing was performed. In this analysis, several assumptions were made: 1: The difference between different grain orientations is only a function of the (relative) direction of the applied stress. This was assumed because the precipitate orientations and the slip planes are well-defined, and their orientations relative to each other would not change with grain orientation. 2: The elastic strain energy on either side of the interface (e.g. matrix versus precipitate) are equal. 3: The precipitates are thin, and therefore elastic strain is uniform throughout the thickness of the precipitate. 4: There is no interaction between adjacent precipitates.

The energy of the interface comes from two major contributions: elastic strain energy and chemical bond energy. Since the interfacial structure is assumed to be uniform in all grain orientations (assumption 1), the chemical bond energy will not change based on grain orientation. Therefore, the elastic strain energy is the term that is the most important. The elastic strain energy term is described using a simple relationship displayed in Equation 29.1.

$$E_{strain}^{ppt} = 2 * \epsilon_0 * C_\gamma * t_p * A \tag{29.1}$$

where E_{strain}^{ppt} is elastic strain energy in the precipitate, ϵ_0 is the lattice mismatch strain (unitless) between the precipitate and the matrix, C_γ is the stiffness component in the direction of the lattice mismatch (MPa), t_p is the thickness over which the strain is acting (units of m), and A is the interfacial area (units of m^2). However, this particular interface is not perpendicular to the orientation of the precipitate as illustrated in **Figure 29.4**. Applying geometry to Equation 29.1 provides:

$$E_{strain}^{ppt} = 2 * \int_0^{x_{max}} \epsilon_0 C_\gamma x D \tan(54)\, dx \tag{29.2}$$

where x is distance in the interfacial direction, x_{max} is the value of x at the edge of the precipitate, and D is precipitate diameter. The applied stress will have an impact based on the angle between the direction of applied stress and the direction of lattice mismatch (θ) such that:

$$f(\theta) = \sum_n \frac{(\cos(\theta) - \nu \sin(\theta))}{n} \tag{29.3}$$

where ν is Poisson's ratio, and the summation term averages this value over the multiplicity of the slip plane orientation, precipitate orientation, and applied stress orientation. This affects the stress at the interface according to Equation 29.4:

$$\Delta\sigma = \epsilon_0 C_\gamma - \left(\epsilon_0 C_\gamma + \sigma_{app} f(\theta)\right) \tag{29.4}$$

where σ_{app} is applied stress, and $\Delta\sigma$ is the change in interfacial stress. Combining these equations provides Equation 29.5.

$$\Delta E_{strain}^{ppt} = 2 * \int_0^{x_{max}} \sigma_{app} f(\theta) x D \tan(54)\, dx \tag{29.5}$$

This value will have an impact on the likelihood that a precipitate will shear or loop. If the deformation behavior of a condition is in a transition between regimes of precipitate shearing and Orowan looping, this value should have

correlation with the strain hardening behavior. A comparison of this value with the strain hardening rate of individual grain orientations in the 200°C overaged condition is shown in **Figure 29.5**. Good correlation exists, which is taken as evidence that strain hardening in this aging condition is controlled by the transition between the two deformation mechanisms.

29.3.2 Interrupted Aging Transmission X-ray Microscopy

Transmission x-ray microscopy experiments were performed at the Advanced Photon Source at Argonne National Laboratory on three alloys: Al-5at%Cu, Al-5at%Ag, and Al-5at%Cu-5at%Ag. Interrupted aging was performed in 1-hour intervals at 350°C in a nitrogen environment to prevent surface oxidation of the small needles. The experiments were successful, but it is difficult to represent the data in 2-D. Additional image processing is underway to provide 3-D images and movies.

29.4 Plans for Next Reporting Period

- Perform additional TEM on 206 Al to observe sheared precipitates;
- Continue data analysis from recent interrupted aging transmission x-ray microscopy experiments of model binary and ternary Al alloys;
- Return to the Advanced Photon Source to perform in-situ transmission x-ray microscopy during aging of model binary and ternary Al alloys;
- Publish creep results in Materials Science and Engineering A or Metallurgical and Materials Transactions A;
- Prepare a publication on 206 Al mechanical property results.

29.5 References

[29.1] S. Roy, L.F. Allard, A. Rodriguez, W.D. Porter, A. Shyam. Comparative Evaluation of Cast Aluminum Alloys for Automotive Cylinder Heads: Part II—Mechanical and Thermal Properties, Metallurgical and Materials Transactions A 48 (2017) 2543–2562.

[29.2] S. Roy, L.F. Allard, A. Rodriguez, T.R. Watkins, A. Shyam. Comparative Evaluation of Cast Aluminum Alloys for Automotive Cylinder Heads: Part I—Microstructure Evolution, Metallurgical and Materials Transactions A 48 (2017) 2529–2542.

[29.3] J. da Costa Teixeira, D. G. Cram, L. Bourgeois, T. J. Bastow, A. J. Hill, C. R. Hutchinson. On the strengthening response of aluminum alloys containing shear-resistant plate-shaped precipitates, Acta Materialia 56 (2008) 6109-6122.

[29.4] J. da Costa Teixeira, L. Bourgeois, C. W. Sinclair, C. R. Hutchinson. The effect of shear-resistant, plate-shaped precipitates on the work hardening of Al alloys: Towards a prediction of the strength–elongation correlation, Acta Materialia 57 (2009) 6075-6089.

[29.5] G. E. Dieter. Mechanical Metallurgy, 3rd Edition, McGraw-Hill, 1988, pp. 103-240.

[29.6] F. R. N. Nabarro. Rafting in Superalloys. Metallurgical and Materials Transactions A 27 (1996) 513-530.

[29.7] S. Koda, K. Matsuura, S. Takahashi. Direct Observation of Interaction of Dislocations with θ′ in an Al-3.8Wt.-% Copper Alloy, J. Inst. Met. 91 (1963) 229–234.

29.6 Figures and Tables

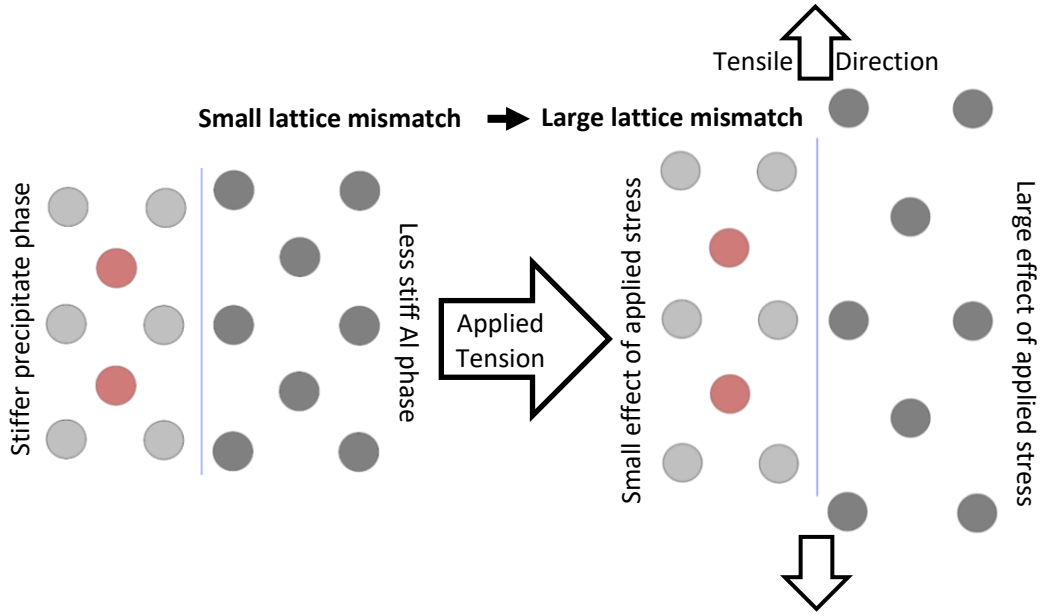

Figure 29.1: Schematic of an elastic mechanism for aggravated lattice mismatch *via* the application of external stress.

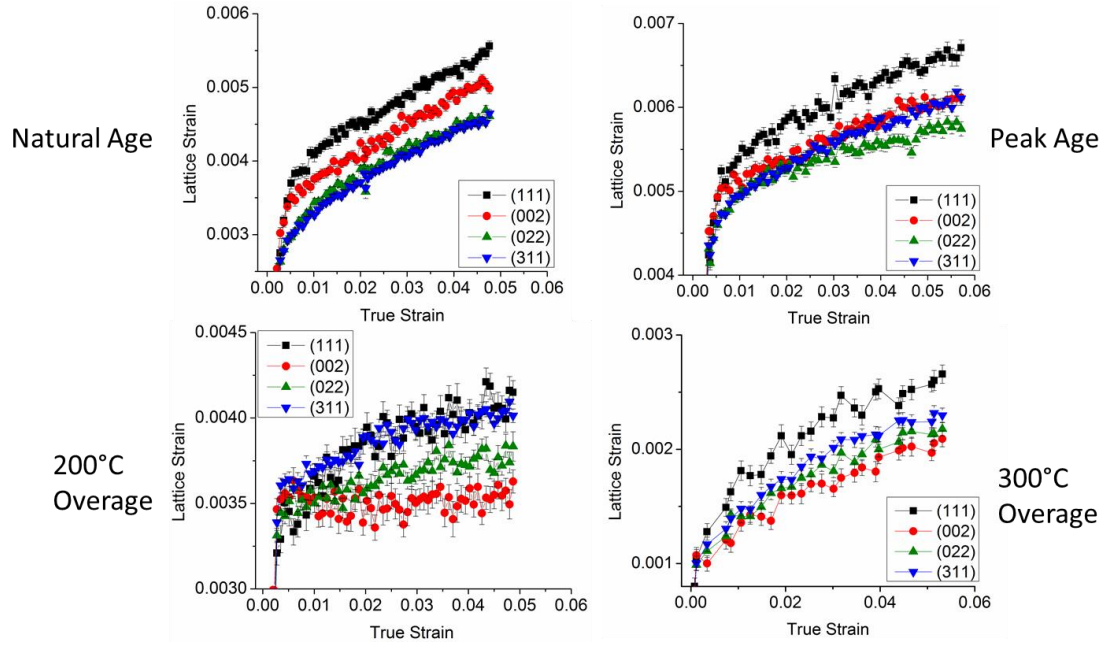

Figure 29.2: Neutron diffraction results for 206 Al showing lattice strain (which is proportional to stress within the crystal) versus macroscopic true strain. Distinct change in deformation mechanisms can be observed as precipitates grow.

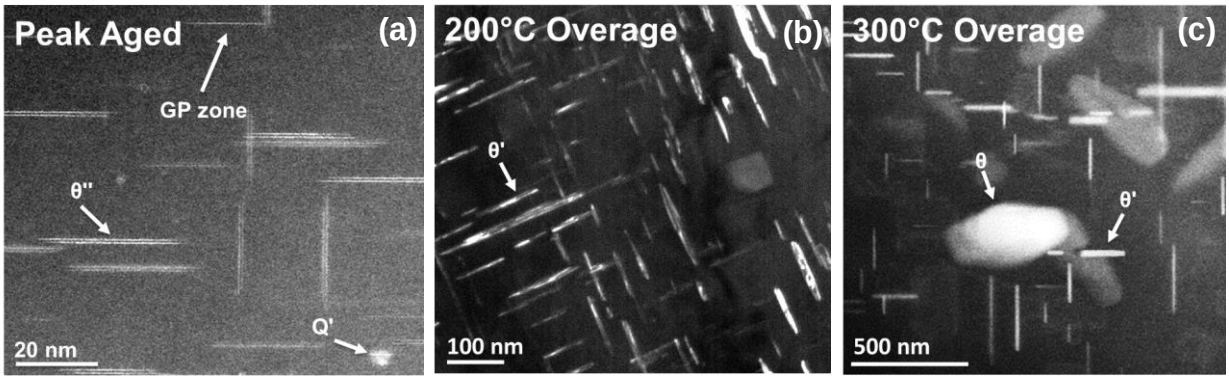

Figure 29.3: STEM-HAADF (a,c) and STEM-DF (b) images of microstructures of Al alloy 206 under various aging treatments. Overaged samples were aged at the given temperature for 200 hours. The naturally aged sample is not shown as the nano-scale precipitates are difficult to image. STEM-HAADF courtesy of L. Allard at Oak Ridge National Laboratory and STEM-DF courtesy of F. Coury at Mines.

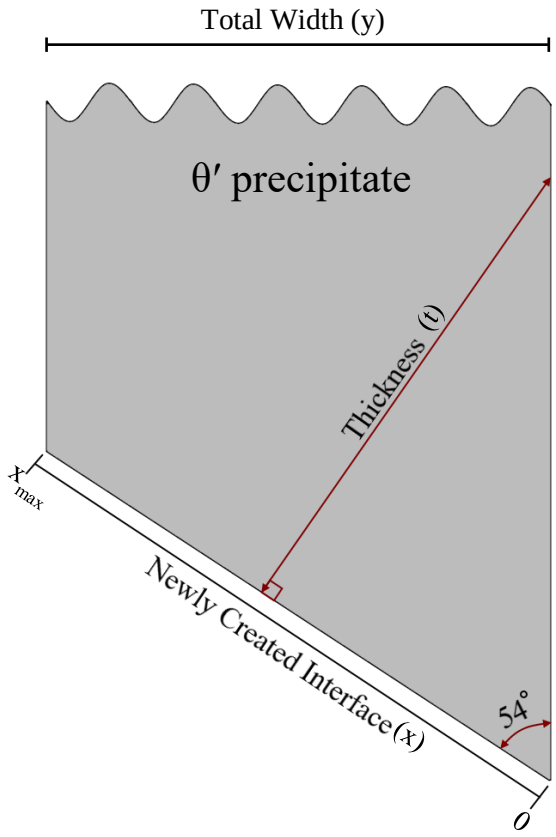

Figure 29.4: Geometry of the interface problem used to develop Equation 2.

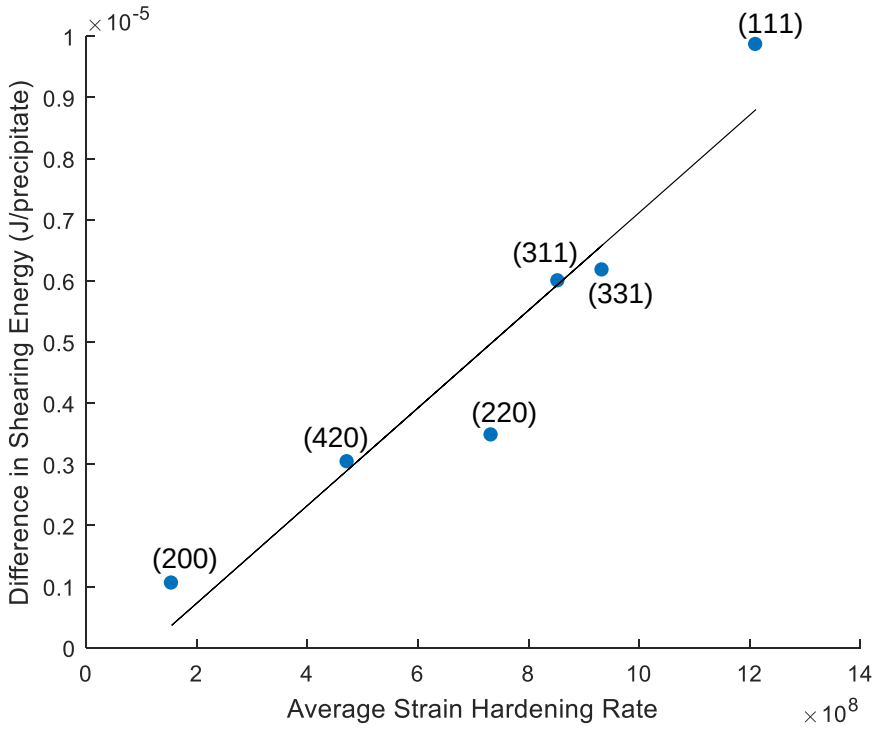

Figure 29.5: Comparison of ΔE_{strain}^{ppt} with average grain orientation specific strain hardening rate in 200°C overaged 206 from 1%-4% strain. Grain orientation relative to the tensile direction are displayed above the points.